ISPRS Journal of Photogrammetry and Remote Sensing 74 (2012) 153–162

Contents lists available at SciVerse ScienceDirect

ISPRS Journal of Photogrammetry and Remote Sensing

journal homepage: www.elsevier.com/locate/isprsjprs

Temporal characteristics of thermal satellite images for urban heat stress and heat island mapping

Janet E. Nichol *, To Pui Hang

Department of Land Surveying and Geo-Informatics, The Hong Kong Polytechnic University, Kowloon, Hong Kong

ARTICLE INFO

Article history:
Received 6 August 2011
Received in revised form 21 April 2012
Accepted 5 September 2012
Available online 5 November 2012

Keywords:
Thermal
Satellite
Urban
Climate

ABSTRACT

The reconstruction of urban climate is still challenging to climatologists in spite of over five decades of research including direct data measurement and model building. Methods for measuring and monitoring urban climate have strengths and weaknesses depending on the application. The mapping of patterns of urban heat stress over a city is not useful if the patterns depicted apply only to the time of data acquisition. Since thermal satellite sensors can now provide detailed temperature data covering whole cities and beyond, their adoption in urban planning depends on demonstrating their relevance to commonly prevailing conditions. This research investigates and presents a methodology based on four summertime ASTER thermal satellite images of Hong Kong for urban heat stress mapping at detailed level. It demonstrates that satellite images obtained under certain climatic conditions, and accompanied by adequate 'in situ' ground data, can provide a basis for an operational heat stress mapping system. The temporal limitation of thermal satellite images is examined for both day and nighttime images by comparison of image-derived air temperatures with ground data representing extended periods and other hot days and nights outside the image acquisition times. The nighttime images were found to be more representative of air temperature at other times than the daytime images, due to a more stable boundary layer, with lower wind speeds and temperature inversion at night. The nighttime images showed high and significant correlations with ground level air temperatures for an average 13-h period surrounding the image time 10.42pm, from 6 pm to 4–8 am the next day. Additionally they were highly and significantly correlated with ground air temperature distributions on 93% of all hot summer nights in the same years. Therefore the nighttime images can be considered representative of a commonly occurring summer nighttime situation in Hong Kong, and can be used to determine the locations of areas where temperatures commonly exceed hot weather warning thresholds. Notably, the images were better able than climate stations to represent areas in the urbanized Kowloon Peninsula and several smaller satellite towns which exceeded hot weather warning thresholds. Many areas exceeded the thresholds, even when no hot weather warning was in force, due to the unrepresentative location of climate stations. The images were also more able than climate stations to indicate the hottest and coolest areas over the Hong Kong territory, thereby enabling measurement of the magnitude and extent of the urban heat island.

1. Introduction

1.1. Hong Kong's urban heat island

Rising global temperatures bring into question the sustainability of tropical and sub-tropical cities (McCarthy et al., 2010), especially those such as Hong Kong where dense and high rise buildings are accompanied by an intense urban heat island (UHI) effect (Fung et al., 2009; Nichol et al., 2009). At 22°N Hong Kong lies at the boundary between the tropics and sub-tropics, experiencing very hot humid summers and warm dry winters. Air temperatures typically reach 33 °C on the hottest summer days, cooling to ca. 26 °C in urban, and 24 °C in rural areas at night, but little research on population heat stress has been done in tropical cities. Dousset et al. (2011) describe the 2003 European heat wave with daytime maxima and nighttime minima exceeding 37 °C and 25 °C respectively over 9 consecutive days, which resulted in 4867 excess mortalities in Paris, and 70,000 over the whole of Europe but mortality appeared to be more closely related to nighttime than daytime temperatures (Robine et al., 2008). In Hong Kong, Kowloon, with a population of over 2 million is the largest continuous urban area and is separated from the rural New Territories by mountain ranges. Parts of Kowloon contain the highest urban population densities in the world, with over 60,000 persons per sq km (Ng, 2009). Reduced ventilation, high temperatures and the blocking

* Corresponding author. Tel.: +852 2766 5952; fax: +852 2330 2994.
E-mail address: lsjanet@polyu.edu.hk (J.E. Nichol).

0924-2716/$ - see front matter
http://dx.doi.org/10.1016/j.isprsjprs.2012.09.007

of sea breezes by tall buildings on newly reclaimed land, the so called 'wall effect' (Wong et al., 2011) are contentious issues. Planners urgently require empirical and spatially comprehensive climatic data to support structure plans and policies but traditional methods of UHI analysis, the use of fixed stations and/or vehicle traverse have been unable to provide such data because the data collected are spatially incomplete.

1.2. Data sources for urban climatic analysis

Data sources for measuring and estimating urban climate include automatic weather stations (AWSs), vehicle traverse, climate simulation models, and satellite observations. However in Hong Kong, as in many other cities, there are no AWS in core city areas, since the Hong Kong Observatory climate station, historically regarded as the most 'urban' is situated in park-like grounds where temperatures are consistently lower than in nearby densely built areas where people live and work. Furthermore, the climatic data used for predicting the effects of temperature on mortality in Hong Kong e.g. number of deaths when the Net Effective Temperature (NET) exceeds 26 °C, are based on temperatures at the (unrepresentative) HKO station. Vehicle traverse data are similarly incomplete spatially, and suffer from a time lag during the data collection. Climate simulation models suffer from the complexity introduced by the roughness of the urban canopy layer structure, the difficulty of mapping surface materials in detail over a city (Herold et al., 2006) and often lack anthropogenic heat contributions (e.g. Ashie, 2007). Additionally most urban climate models represent local (i.e. urban canyon) scale processes (Mills, 1993; Arnfield and Grimmond, 1998; Arnfield, 2000), or neighborhood scale processes (Grimmond et al., 2010) which are difficult to scale up to land use zones or whole cities. Thus they do not easily predict temperature patterns at city scale, or permit studies of urban heat islands. Very recent developments in CFD modeling are able to simulate energy balance and air temperatures across a whole city, but use very large databases and are highly computer intensive (Ashie and Kono, 2011). Other recent developments include the downscaling of regional climate models such as WRF to city and district scale (Chen et al., 2011), but they incorporate limited land cover types e.g. the WRF urban modeling system incorporates only three land cover types.

Complete and time-synchronous coverage of an urban area can be obtained from thermal infrared satellite sensors which measure surface temperature (T_s), thus the locations of the actual maximum and minimum surface temperatures over a city region can be obtained (Johnson et al., 1993) and intra-urban thermal patterns can be observed. A variety of airborne and spaceborne sensors are used for measurement of the urban surface, which climatologists regard as the 'source area' for air temperature measurements (Schmid, 1997).

The turbulent source area for air temperature is a patch of the surface upwind from the air temperature sensor from which parcels of air that are measured by the sensor acquire their thermal properties (WMO, 2008; Murphy et al., 2011). However, the satellite (radiative) source area corresponds to the upwelling thermal radiance from within the IFOV. The surface area 'viewed' by the satellite is also directional, and subject to anisotropy (Voogt and Oke, 1997; Nichol, 1998) and shadowing effects in high rise areas. Both these factors create a mis-match between the source area of a particular pixel (i.e. the surface 'seen' by that pixel) and the air measured adjacent to it. Factors most influential in the relationship between surface and air temperature have been recognized as atmospheric mixing, wind velocity and the characteristics of surface materials which influence heat flux (Stoll and Brazel, 1992; Voogt and Oke, 2003). The practical application of satellite-derived temperature data is also limited by the uncertainty of their relevance to times and dates other than the immediate imaging time, especially in cloudy regions where good quality thermal images may be obtained only infrequently. In summary, the satellite-derived surface temperature may be able to represent air temperature, and its relevance is dependent on the establishment of a robust relationship between the surface and adjacent air at the image time. If this relationship can be demonstrated to be temporally stable, and representative of other times and dates where commonly occurring climatic conditions occur, it is suggested that the image can be used as a working model of the spatial distribution of air temperatures over a city for planning purposes.

1.3. Objectives

This research tests the relevance of temperature patterns observed on thermal satellite images both at the image time, and at other times based on Stoll and Brazel's (1992) assertion that correlations between surface and air temperatures are dependent on atmospheric mixing, mean wind velocity and the thermal properties of surface materials. Thus, on imagery obtained during a stable atmosphere and low wind speeds (e.g. at night, when turbulence is greatly reduced (Kawashima et al., 2000; Voogt and Oke, 2003)), and surface effects minimized, reduced advection would result in a stronger relationship between the surface and the adjacent air. Thus the image may provide a representation of air temperatures accurate enough for a working model of a city's urban heat island situation. For example Fung et al. (2009) observed an R^2 of 0.78 between over 14,000 air temperature points from a mobile vehicle traverse, and a night-time ASTER thermal image, when ground measured air temperature points falling within the same pixel were averaged. The temporal deficiency of satellite images, being acquired at a single point in time is also likely to be minimized under such conditions, when heat island patterns depicted may persist for several hours, although this has not been tested previously. It is relevant because UHI patterns present under a stable atmosphere may represent a typical, or baseline heat island situation for a city i.e. a heat island distribution pattern which is the most commonly prevalent.

In light of the urgent need for information in Hong Kong discussed above, this study uses a daytime and a nighttime ASTER thermal satellite image of Hong Kong's urban areas with 'in situ' field measurements of surface and air temperatures to examine the extent to which satellite-derived land surface temperatures (LSTs) can represent a spatial pattern of air temperatures most prevalent across a city. Extended periods beyond the image time which typify the character of the city's temperature distribution are examined, to provide a basis for an intra-urban heat stress mapping system based on 'very hot day' and 'very hot night' thresholds. This is conducted both at the detailed level of sub-districts and street blocks, as well as the macro-scale required for UHI analysis.

2. Study area

The whole of the Hong Kong Territories, with a population approaching 7 million and approximately 1067 sq km land area was selected for the study, but emphasis was placed on the largest urban area, the Kowloon Peninsula with a population of 2.2 million and land area of 47 sq km. Kowloon mainly consists of high-density residential areas, commercial districts and urban parks. The topography is flat in the southern part and hilly in the northern part where elevation ranges from 3 m to 200 m. Several smaller satellite towns with population approximating 500,000 have been established in the New Territories, to the north and west of Kowloon. At the time of the daytime image (11.09 am local time) the

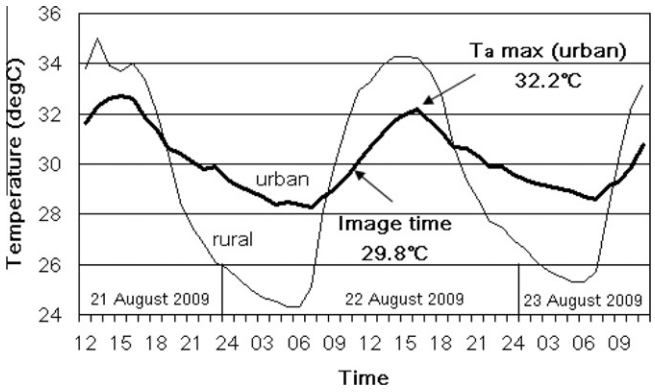

Fig. 1. Air temperature at the Hong Kong Observatory (urban) and T_a Kwu Ling (rural) climate stations for the 48 h surrounding the daytime image time.

atmosphere was unstable with a PBL height of 1300 m (from morning and evening radiosondes at the Hong Kong International Airport (HKIA)), wind speeds were medium to high at 3–4 ms west-southwesterly, and relative humidity fairly high, at 72%. Fieldwork at 61 sites in urban areas including Kowloon and several small towns (Section 3.2) indicated that mean surface temperature had risen to 10–20 °C above mean air temperature of 33–36 °C. Interestingly, air temperature at the Hong Kong Observatory's 'urban' climate station was only 29.8 °C (Fig. 1), which is considerably lower than the field measurements, probably due to its location in park-like grounds where a morning lag in warming may be expected. Thus temperatures at the image time would not have qualified as a 'hot day' (above 30 °C). The definition of hot days and nights follows the Hong Kong Observatory (HKO)'s criteria (Leung and Yeung, 2004; Leung et al., 2008) of bio-meteorological indicators for the local population, as follows:

Very Hot Day	*Ta maximum*	⩾33 °C
Hot Day	*Ta maximum*	⩾30 °C
Very Hot Night	*Ta minimum*	⩾28 °C
Hot Night	*Ta minimum*	⩾25 °C

and generally, hot weather warnings are issued for 'very hot day' or 'very hot night' conditions.

For the nighttime image the atmosphere was stable with PBL height (from the morning and evening radiosonde at HKIA) of 65 m and low wind speeds of less than 1 ms, southwesterly. Relative humidity moderate, at 72%. Field measurements indicated that, by the image time 10.42 pm, mean surface temperatures in urban areas had fallen close to air temperatures at 28–30° which is similar to the HKO reading (Fig. 2). This did not qualify as a 'Hot Night' as minimum temperatures at HKO fell below 28 °C later that night (Fig. 2).

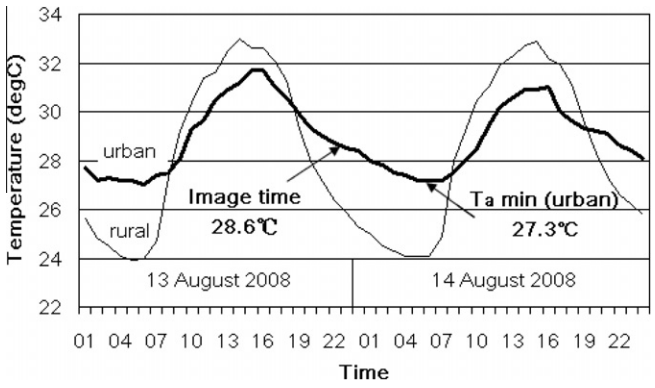

Fig. 2. Air temperature at the Hong Kong Observatory (urban) and T_a Kwu Ling (rural) climate stations for the 48 h surrounding the nighttime image time.

It is important to note that the image times do not correspond to either temperature maxima or minima which are used in many heat stress indices, or to the UHI maximum i.e. the time of greatest difference between urban and rural temperatures (Figs. 1 and 2).

3. Methods

3.1. Data and processing techniques

Two ASTER Level 1B images at 90 m resolution obtained at 11.09 am on 22nd August 2009, and 10.42 pm local time on 13th August 2008 respectively, were registered to the HK1980 coordinate system by referencing the control points on the images to the corresponding points on a coastline vector file and root mean square errors (RMSE) for both images of less than 0.5 pixel were obtained. The digital number (DN) values of the images were converted to radiance using the unit conversion coefficient of 5.693×10^{-3} (ERSDAC, 2010). After obtaining the radiance, black body temperature (BBT) was computed using Eq. (1) derived from the inversion of Planck's function (Jensen, 2007).

$$T_{BBT} = \frac{c_2}{\lambda \cdot \ln\left(\frac{c_1}{\lambda^5 R} + 1\right)} \quad (1)$$

where T_{BBT} is the black body temperature, c_1 is the first radiation constant for spectral radiance (1.191×10^{-6}), c_2 is the second radiation constant (1.438×10^{-2}), λ is the wavelength of Band 13 (10.55 μm) and R is the radiance.

To correct for emissivity differences of surface materials, an emissivity map was produced from an existing 10 m resolution digital land cover map with six broad land cover classes, namely forest, water, grassland, shrubland, urban, and soil/sand. The land cover classes were converted to a 10 m emissivity image by allocating the emissivity values to the land cover classes, with the emissivity values from spectral libraries. The correction of the T_{BBT} image for the emissivity differences of different land covers was done using Eq. (2) (Sabins, 1997; Nichol, 2009), which is an approximation of the true equation. Thus the 90 m blackbody temperature image was converted to a T_s image at 10 m resolution, where

$$T_s = \frac{T_{BBT}}{\varepsilon^{\frac{1}{4}}} \quad (2)$$

where T_s is land surface temperature, and ε is the emissivity value. The procedure is known as emissivity modulation rather than absolute emissivity correction, since it is assumed that temperatures within a large pixel vary only by cover type. Thus the emissivity correction modulates the thermal values within the larger pixel block, but some distortion may be expected, since the temperature value of a small output pixel will still be influenced by the *Tb* values of surrounding cover types in the original lower resolution pixel block. This distortion would be greater for fragmented cover types

In order to validate the accuracy of the emissivity values used, the ASTER emissivity image product AST09 for the daytime image derived from the ASTER TES algorithm (Gillespie et al., 1999) was used for comparison. The validation was done by correlating the 90 m ASTER emissivity image with the derived 10 m emissivity image. A very strong correlation of $R^2 = 0.99$, with slope and offset of 1 and zero respectively, was observed between 90 m ASTER emissivity images and our derived 10 m emissivity image.

3.2. Fieldwork

For each image, 'in situ' air and surface temperatures were collected over a 3-h period centered on the image time. Locations included urban centers, new towns and rural areas all over the Hong

Table 1
Nighttime field data used for air temperature conversion, and night and daytime AWS data used for verification of the image-derived temperatures, showing degree of urbanization from most urban (1) to least urban (7) according to Oke (2004). The 61 field locations for the daytime image are too numerous to list, but have similar wide distribution among degrees of urbanization.

Night field data			Night AWS data			Daytime AWS data		
Station	Air temp	Urban zone	Station	Air temp	Urban zone	Station	Air temp	Urban zone
Yuen Long Park (grass)	27.9	6	Tsuen Wan	26.9	7	Ching Pak House	30.1	5
Yuen Long Park (concrete)	28.3	6	Kow Sai Chau	26.2	7	HKO	30.1	6
Yuen Long Park (leaf)	28.2	6	Sheung Shui	27.5	6	King's Park	31.2	6
Yuen Long Stadium (concrete)	29.2	4	Wetland Park	27.4	7	Sheung Shui	32.1	6
Yuen Long Stadium (concrete)	29.1	4	Sai Kung	27.8	4	Ta Kwu Ling	32.9	5
YMT Temple Street (brick)	29.5	1	Shau Kei Wan	27.9	7	Ho Koon Education Centre	30.1	7
YMT Temple Street (grass)	29.6	1	Ching Pak House	27.8	5	Queen's College OB Ass Sec Sch	31.2	2
Castle Peak (Kwai Chung) (concrete)	28.6	6	Kowloon City	27.8	7	Fung Kai LMST Secondary Sch	31.9	2
Tsuen Wan City Hall (concrete)	29.2	1	Tai Po	28.4	7	Ju Ching Chu Secondary Sch	31.7	2
Tsuen Wan City Hall (brick)	29.6	1	King's Park	28	6	HKCCCU Logos Academy	31.5	2
Ma On Shan Police Station (concrete)	29.2	3	HKO	28.5	6	SKH Kei Fook Primary School	32.7	1
						Sing Yin Secondary Sch	32.8	2

Kong Territory. Each team was equipped with a data logger thermometer with a TPK01 beadprobe thermocouple wire (which minimizes the radiation error for daytime sampling), and a TPK-04L surface temperature probe, both with accuracy of 0.1 °C, which had previously been calibrated using boiling water and ice. An average of three air temperature readings were made, at one meter above the surface, and all air temperatures derived in this study refer to this height level. A range of surface materials was selected. The coordinates of the field sites were recorded by GPS for easy comparison with the 10 m image pixel coordinates.

3.3. Air temperature conversion

As thermal satellite sensors measure T_s it is necessary to convert this to air temperature since most urban climate research refers to air temperature (e.g. thermal comfort, UHI, etc.). The air temperatures measured at 61 (daytime) and 11 (nighttime) points in the field (Table 1) within 1.5 h of the image time were regressed against the T_s value of the corresponding image pixel (Eqs. (3) and (4)). The corresponding R^2 between T_s and T_a are 0.74 ($n = 61$) for daytime and 0.82 ($n = 11$) for nighttime (Fig. 3), and the significant R^2 values suggest air temperatures measured in the field are suitable for converting T_s to air temperature.

$$\text{Daytime } T_a = 0.52^{*}T_s + 14.027 \quad (3)$$

$$\text{Nighttime } T_a = 0.23^{*}T_s + 20.198 \quad (4)$$

This direct conversion of T_s to T_a does not require atmospheric correction of the image surface temperatures, since surface temperature was not required, and many 'in situ' screen level (bottom of atmosphere) air temperatures were available, both for building the regression equation as well as for validation.

The image-derived air temperatures were validated by correlating with 12 (daytime) and 11 (nighttime) AWS at 1.5 m above ground at the time of imaging (Fig. 4) (Table 1). An R^2 value of 0.75, and Mean Absolute Difference (MAD) of 3.57 °C were obtained for daytime and an R^2 value of 0.84 and MAD of 1.4 °C for nighttime were obtained. Both R^2 statistics are significant at 5% level, which suggests that the two satellite images are suitable for studying patterns of air temperature distribution over Hong Kong. The large MAD for the daytime image is thought to be due to the situation of many of the AWS generally in building shade, or in treed park-like grounds such as at the HKO station (Table 1), and which, due to anisotropic effects, are 'unseen' by the satellite. The morning heating of these sites may lag behind the more open urban sites used for field measurements by several degrees. The difference for nighttime, though smaller, has a similar explanation. Table 1 indicates that most AWS sites were either rural or sub-urban (column 6) compared to the more urbanized fieldwork sites (column 3).

3.4. Hourly and daily analysis

The images are deemed more relevant if they can represent temperature patterns at other times of the 24-h cycle, especially the times of maxima and minima used for measurement of heat stress, and on days other than the image date. Therefore, to determine the hourly relevance the temperatures recorded several hours before and after the imaging time at 12 (daytime) and 11

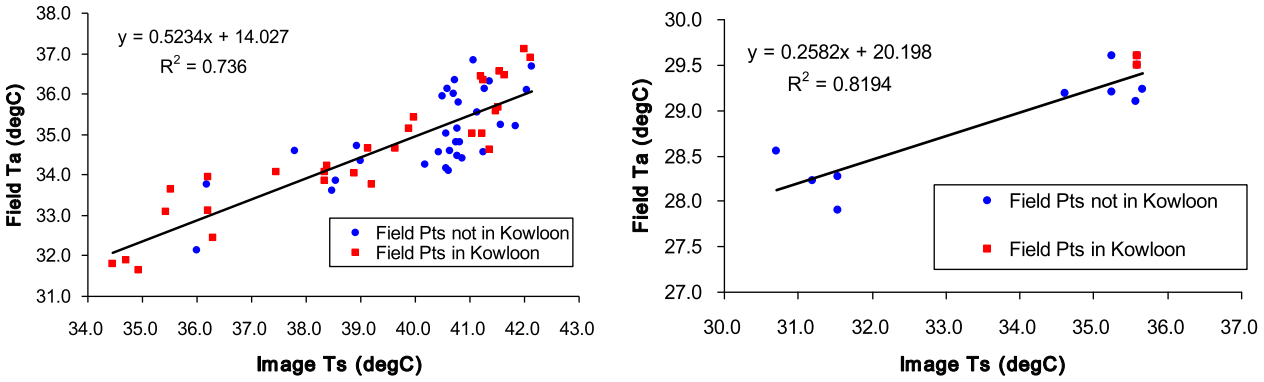

Fig. 3. Air temperatures (T_a) from field measurement approximately 1 m above the ground at image time, for daytime image (left) and nighttime image (right), compared with (T_s) from corresponding image pixel values.

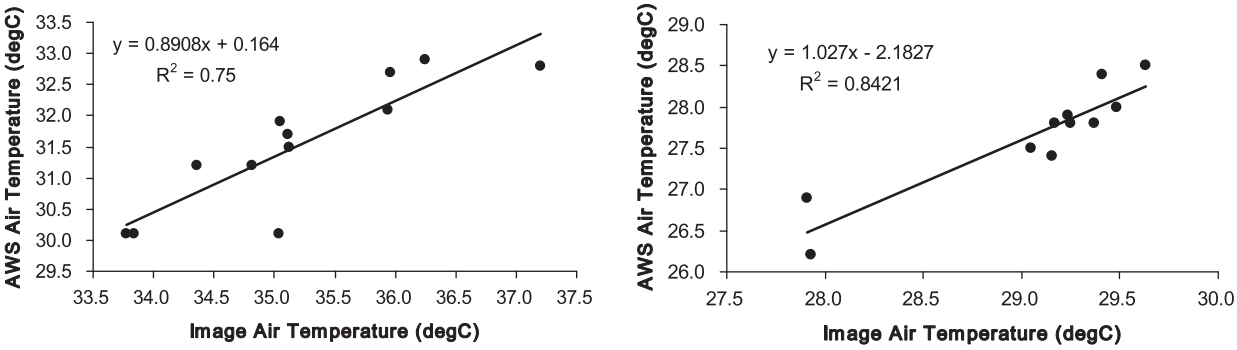

Fig. 4. Daytime (left) and nighttime (right) image-derived air temperatures, and the AWS air temperatures used for validation.

(nighttime) AWS were correlated with the image-derived air temperature.

Daily analysis was conducted by correlating the image values with the AWS temperatures recorded at the image time on other days with similar atmospheric conditions to the image date, for the summer season between July and September of the same year. Days fulfilling the following requirements were selected for the analysis: for the daytime image T_aMax was not below 30 °C, and for the nighttime image T_aMin was not below 25.5 °C and for both, severe typhoon warnings should not have been issued. These conditions would include all dates similar to those on which the images were collected i.e. all hot summer days and nights, and exclude significant rain events such as typhoons when temperatures are lower and climatic conditions unstable.

To strengthen the investigation of temporal relevance, two additional images of 13 September 2008 and 17th September 2009, for day and night respectively, were similarly processed, and also correlated with hourly and daily air temperature patterns. Results for all four images are therefore given in Sections 4.1 and 4.2, but due to the late summer (September) date of the second set of images they were not used in heat stress mapping (Section 4.3).

4. Results

In Sections 4.1 and 4.2, figures in brackets refer to the second set of images used in the temporal analysis, i.e. September 2008 for daytime and September 2009 for nighttime.

4.1. Hourly analysis

Fig. 5 shows that the correlation between the daytime image-derived and AWS air temperatures peaks at the imaging time of 11.09 am with R^2 of 0.75 (0.63), but with a second peak in the afternoon (R^2 of 0.74) for the September 2008 image. For the period 9:30 am to 1:30 pm (7.30 am to 9.30 pm but excluding 2 pm) surrounding the image time, the p-values indicated that correlations are significant at 5% level indicating that the daytime image can effectively represent the temperature distribution for a 4 (10)-h period, surrounding the imaging time. The nighttime correlations also peak at the image time 10.42 pm, with R^2 = 0.84 (0.85), and remain relatively steady (R^2 around 0.7) approximately 3 (2) h before, and 2 (3) h following the image (Fig. 6). However, the results are significant for a 10 (16)-h period from 6 pm to 4 (9) am of the next day, which is 6 (5) h longer than for daytime. A possible reason for the much longer period of validity at night observed on both images is that convection and advection subside at night producing a stable atmospheric environment (Dousset, 1989; Johnson et al., 1991). Additionally, the directional radiance within the sensor IFOV is less influenced at night by uneven patterns of solar illumination in high rise areas.

4.2. Daily analysis

Seventy-six (69) dates for daytime and 69 (66) for night were able to satisfy the set criteria for similarity of weather conditions. Of the 76 (69) daytime dates, only 17 (29) were significant at the

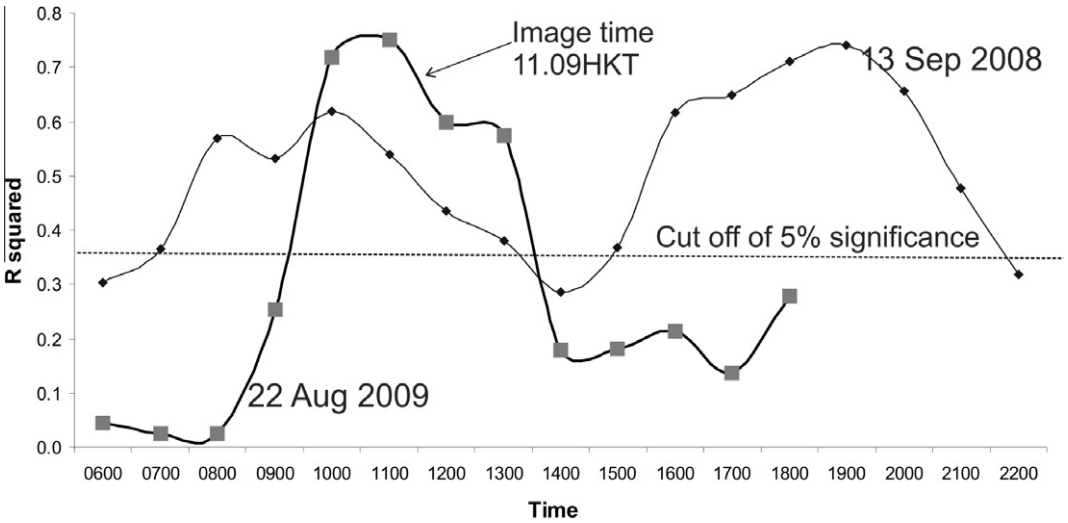

Fig. 5. Hourly time series correlation analysis between image-derived and 12 AWS recorded air temperature on two daytime images.

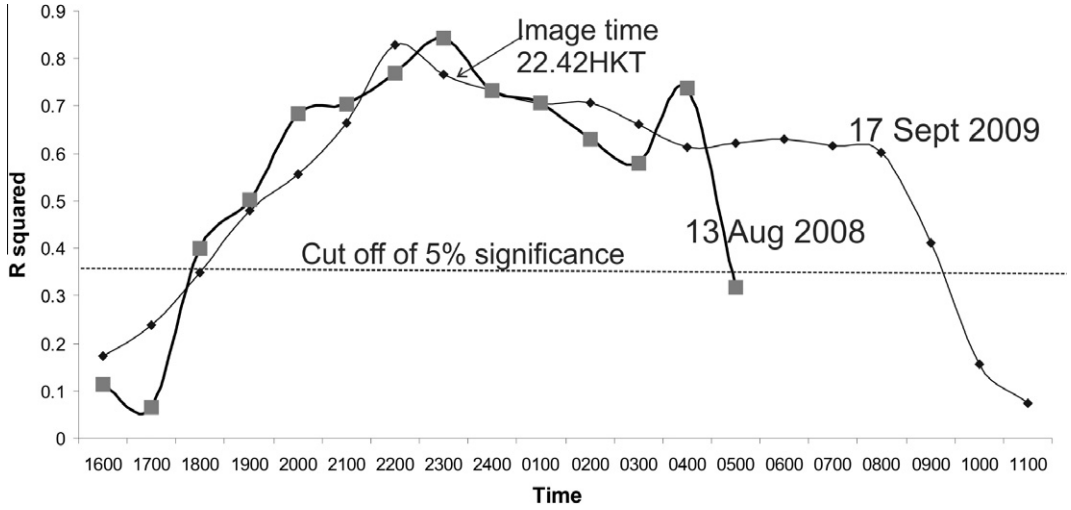

Fig. 6. Hourly time series correlation analysis between image-derived and 11 AWS recorded air temperature on two nighttime images.

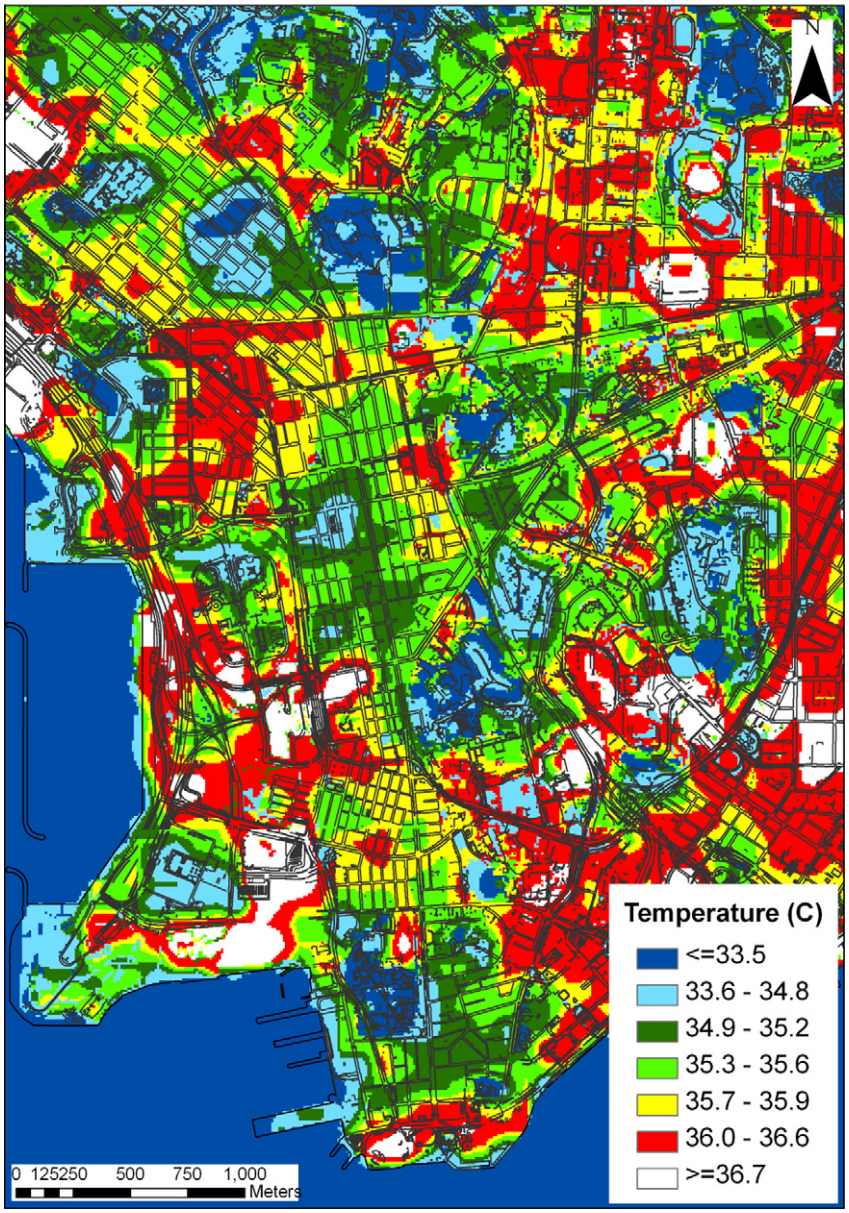

Fig. 7. Summer mid-morning air temperature image of the Kowloon Peninsula derived from Eqs. (1) and (2), with street network superimposed.

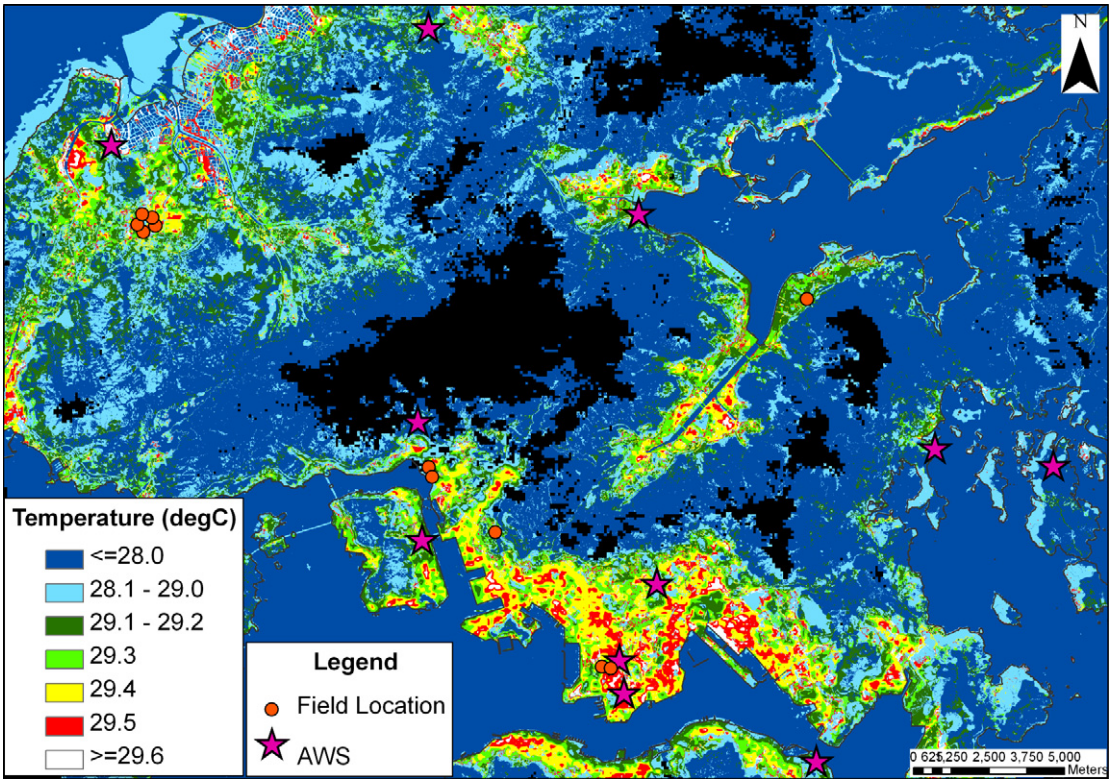

Fig. 8. Summer nighttime (10.40 pm) air temperature image of Hong Kong derived from ASTER. The urbanized Kowloon Peninsula is at lower center, and shows the highest temperatures, but some smaller satellite towns farther north and west also show significant heat islands. Locations of the 11 field air temperature measurements and 11 AWS used for the nighttime image are shown. The 61 field locations for the daytime image are too numerous to depict clearly but have similar wide distribution between rural and urban areas.

5% level, with a mean R^2 value of 0.22 (0.32), but for the nighttime image 62 out of the 69 dates were significant with some very high R^2 values above 0.9, and an average R^2 of 0.6 (0.62). Even on 20 August 2008 when a typhoon was centered near Hong Kong the correlation was significant at $R^2 = 0.56$. The good and significant correlations for nights other than the imaging dates, for both images covering the summers of 2008 and 2009, suggest that images obtained on representative dates with typical seasonal weather conditions (in this case cloud-free night with low wind speeds, with strongly developed UHI) can be used to retrieve temperature patterns on many other days within that season. The much higher nighttime R^2 values indicate that nighttime images are better able to account for temperature patterns observed on other days, than are daytime images.

4.3. Heat stress mapping

Areas of heat stress on the image can be mapped. For the daytime image Fig. 7 indicates that air temperature had already reached 35 °C in late morning over most of the urban area (represented by light green, yellow, red[1] and white colours in Fig. 7), which would be classified as a 'Very Hot Day' ($\geqslant$33 °C), although at the HKO climate station air temperature was below 30 °C (Fig. 1), thus not even qualifying as a 'Hot Day'. Maximum temperatures were reached at 3 pm that day, with 32.2 °C at HKO which would not have qualified for a hot weather warning (T_aMax > 33 °C) (Fig. 1). Although it is likely that the areas of the image above 35 °C in Fig. 7 would have exceeded 37 °C by 3 pm, the spatial distribution is uncertain since the daytime image values were only significant between 9.45 am and 1.30 pm.

The nighttime image however significantly depicts air temperature distribution for a 10-h period including the critical nighttime T_a minimum at 4 am. A decrease in T_a of 1.3 °C between the image time at 10.42 pm and 4 am according to the temperature curve for HKO (Fig. 2) would identify the top three temperature classes (yellow, red and white in Figs. 7 and 8) to be classified as 'Very hot night' as they remained above the hot weather warning threshold with T_aMin above 28 °C. In fact the more open HKO site is likely to have cooled faster than the more urbanized regions at night, so the prediction of 'Very Hot Night' for the urban areas is a least case scenario. These areas which cover most of the urban areas of Kowloon and small towns in the New Territories (Fig. 8) constitute localized 'very hot nights'. Interestingly, no hot weather warning was announced over that day or the previous 24 h since, as Fig. 2 shows, the HKO station recorded T_aMax below 33 °C and T_aMin below 28 °C, thus no hot weather warning was issued in either daytime or nighttime. The significant relationship between the image date and 90% of other hot summer nights enables the identification of specific local neighbourhoods of the city which suffer heat stress on a regular basis, and in this case, on most summer nights.

5. Discussion and conclusions

In this paper, two daytime and two nighttime thermal satellite images were examined, and found to be capable of representing spatial patterns of Kowloon's UHI for an average of 7.5 and 13 h on the imaging day, respectively, and an average of 23 and 64 days in the same imaging season. The nighttime images were particularly representative of the summer nighttime UHI in Hong Kong, as the image temperatures were significant on 125 out of 135 nights tested over the two summers of 2008–9. These represented 93% of the hot summer nights in those years. The relevance and

[1] For interpretation of colour in Figs. 3 and 10, the reader is referred to the web version of this article.

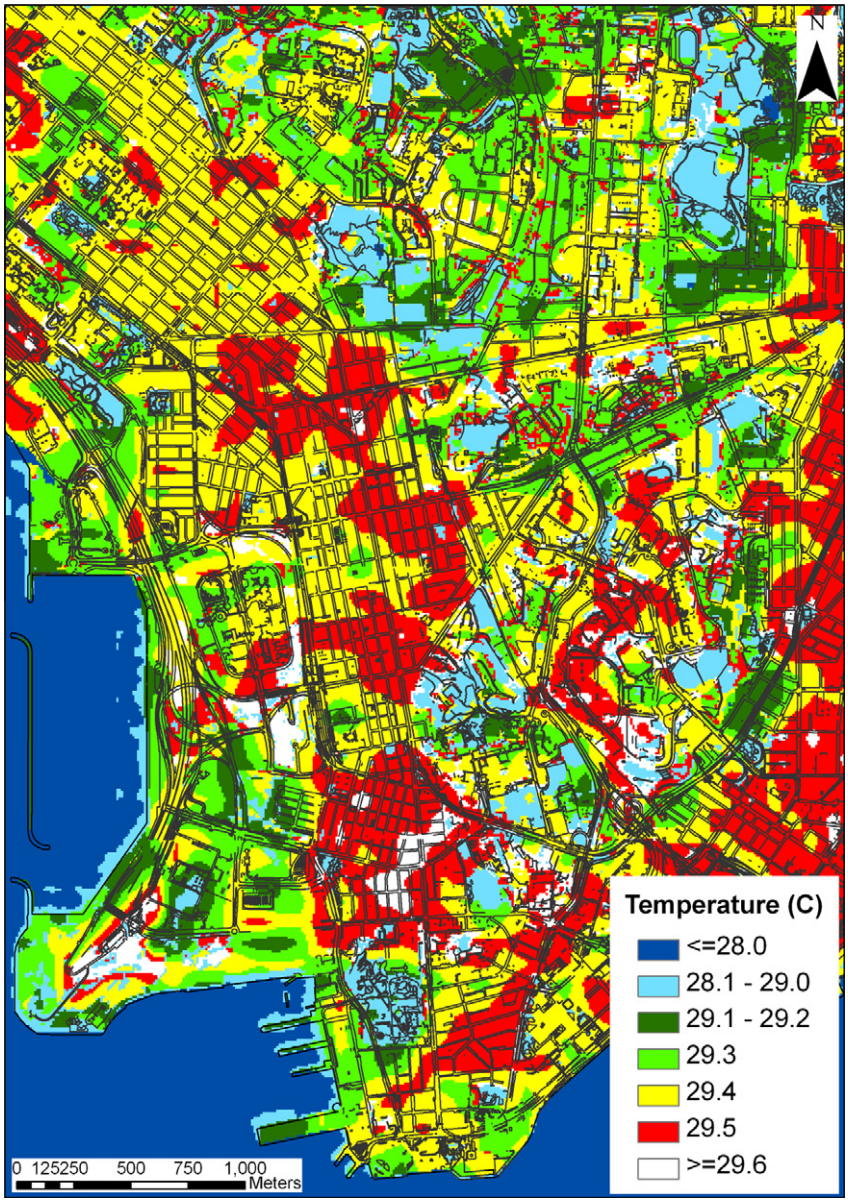

Fig. 9. Summer nighttime air temperature image of the Kowloon Peninsula at 10.42 pm derived from Eqs. (1) and (2), with street network superimposed.

applicability at times other than the immediate image time is to some extent expected in view of the dominant roles of street canyon geometry and the thermal properties of surface materials on urban climatology (Johnson et al., 1991; Oke et al., 1991) because these factors are constant over time. However they are most influential at night on calm cloudless nights when the UHI is best developed (Johnson et al., 1991). In Hong Kong, for the August nighttime image, atmospheric stability within the urban canopy layer was reinforced by the presence of a temperature inversion at 65 m. The more stable atmospheric conditions prevailing at the nighttime situation are typical of summer nights in Kowloon. In summer several hours after sunset, similar land and sea temperatures minimize sea breezes and the dense urban structure compounded by the 'wall effect' (Wong et al., 2011) further reduce wind speeds. It is thought that the source areas for the image-derived air temperatures in this study would have been much more local and possibly within a few 10s of meters, which corresponds to a few pixels. This is because the air temperatures were measured at only 1 m height, with low wind speeds of less than 1 ms. For comparison purposes, Murphy et al. (2011) observed that for a 10 m high air temperature sensor and moderate wind speeds from 3 to 5 ms, the best fit upwind fetch wedge was found to be at 180 m distance. A further reason for the high correlations may be due to the absence of temporal variation due to solar heating, meaning that if the correlation is good at one point in time at night it will likely also be quite good at other times. Thus the images of 13th August 2008 and 17th September 2009 may be considered representative of a commonly occurring summer night-time situation of the urban heat island in Kowloon, especially in the hottest part of the summer, on days when rainy or typhoon conditions are absent.

The close correspondence of the image air temperature patterns, both at the image time and other times and dates, to those recorded at AWS permits the mapping of areas where temperatures persistently exceed biometeorological thresholds defined for the local population. The August daytime image is less applicable at other times due to greater turbulence within the urban canopy layer in the daytime, as well as possibly some anisotropic effects of the image viewing, and sun angles. However the image does indicate that, by the image time 11.09 am, all urban areas in both Kowloon and small satellite towns far exceeded thresholds

Fig. 10. Extract from Fig. 9 showing streets at Kowloon's heat island core (white area) with air temperatures above 29.6 °C at the image time 10.42 pm. The core area occurs where Temple Street, Woosung Street and Parkes Street intersect the east–west oriented Bowring Street, in the area regarded as Chinatown, with high buildings, and narrow and congested walkways.

for 'very hot day' and for issuance of a hot weather warning, although temperature at the 'urban' climate station used for official determination of weather warnings was currently well below the threshold level of 33 °C.

Since air temperature patterns depicted on the nighttime image are significant at the time of T_aMin used for determining hot nights and hot weather warnings, the image provides strong evidence of the shortcomings of the current hot weather warning system. It depicts most urban areas in Kowloon and smaller satellite towns as having T_a exceeding the threshold of 28 °C when extrapolated to the time of T_aMin, whereas no hot weather warning was issued on that date. Thus the main urban weather station operated by the Hong Kong Observatory's urban climate station, located in treed park-like surroundings does not represent temperatures in the hottest districts which are usually several degrees higher in the daytime and one or two degrees higher at night. Nighttime heat is more dangerous as most of the cardiovascular diseases are triggered at night (Vandentorren et al., 2006; McCarthy et al., 2010). It is also the critical time in heat-stress related morbidity because of the inability to cool down over the 24-h period (Pascal et al., 2006). Therefore the nighttime image is very useful for identifying areas where populations are at risk of heat-related sickness or mortality.

Furthermore, the nighttime image is able to locate areas of temperature maxima and minima, unlike automatic weather stations which are sparsely distributed, and due to historical reasons not located in either dense urban or truly rural districts. Thus it is capable of depicting the magnitude and spatial distribution of the UHI over the whole of the Hong Kong territory, including both Kowloon with population over 2 million, and smaller towns with population around 0.5 million. The image also suggests that the magnitude of the UHI is not related to settlement size, as noted by some previous studies where larger cities had greater UHI intensities measured by vehicle traverse (Oke, 1973; Park, 1986; Yamashita et al., 1986). Fig. 8 shows several small satellite towns in the New Territories which occupy the same range of temperature classes as the much larger Kowloon urban area. In addition to the coverage of a whole city and beyond, which is not available from other methods of urban climate measurement, or from urban climate models, the image depicts T_a at a detailed level such that temperatures at street scale can be determined. For example Fig. 10 shows an enlarged section of Fig. 9, including streets in Jordan and Yau Ma Tei, older urban districts of Kowloon, where high built density combined with medium rise buildings of 10–12 floors contribute to low sky view factors. The hottest areas (white and red areas in Fig. 10)

can be seen to correspond very closely to the densest street network (at center left), with low sky view factor. Temperature sensors for an urban heat stress warning system would ideally be located in such an area. In order to mitigate nighttime heat stress, urban renewal may consider increasing open/green space at ground level to improve ventilation, while maintaining plot ratios by increasing the number of floors.

These assertions regarding weather warning thresholds based on image observations are dependent on the absolute accuracy of the image temperatures, which is based on the regression between the image and 'in situ' air temperatures at the image time. Therefore, substantial 'in situ' ground-measured air temperatures are essential for air temperature calibration and validation. The method is recommended for nighttime situations when the images are more able to represent commonly prevailing air temperature distributions than during the day, due to both climatic and image-based factors.

Acknowledgments

The authors would like to acknowledge Mr. Olympian Kwok for technical support in processing the images. Grants 5006-PPR-09 and PolyU 5264/08E supported this research.

References

Arnfield, A.J., 2000. A simple model of urban canyon energy budget and its validation. Physical Geography 23 (1), 305–326.

Arnfield, A.J., Grimmond, C.S.B., 1998. An urban canyon energy budget model and its application to urban storage heat flux modelling. Energy and Buildings 27, 61–68.

Ashie, Y., 2007. Numerical simulation of urban heat island in a 10-km square area of central Tokyo. In: Annual report of the Earth Simulator Center, Japan Agency for Marine Earth Science and Technology. ISSN: 1348-5822.

Ashie, Y., Kono, T., 2011. Urban-scale CFD analysis in support of a climate-sensitive design for the Tokyo Bay area. International Journal of Climatology 31 (2), 174–199.

Chen, F., Kusaka, H., Bornstein, R., Ching, J., Grimmond, C.S.B., Grossman-Clarke, S., 2011. The integrated WRF/urban modelling system: development, evaluation, and applications to urban environmental problems. International Journal of Climatology 31 (2), 273–288.

Dousset, B., 1989. AVHRR-derived cloudiness and surface temperature patterns over the Los Angeles area and their relationship to land use. In: Proceedings of IGARSS-89 (2132–2137), New York, IEEE.

Dousset, B., Gourmelon, F., Laaidi, K., Zeghnoun, A., Giraudet, E., Bretin, P., Mauri, E., 2011. Satellite monitoring of summer heat waves in the Paris metropolitan area. International Journal of Climatology 31 (2), 313–323.

Earth Remote Sensing Data Analysis Centre (ERSDAC), ASTER GDS, 2010. <http://www.gds.aster.ersdac.or.jp/gds_www2002/exhibition_e/a_sensor_e/set_a_sensor_e.html> (accessed 04.07.11).

Fung, W.Y., Lam, K.S., Nichol, J.E., Wong, M.S., 2009. Heat Island study – satellite derived air temperature. Journal of Applied Meteorology and Climatology 48 (4), 863–872.

Gillespie, A.R., Rokugawa, S., Hook, S., Matsunaga, T., Kahle, A.B., 1999. Temperature/Emissivity Separation Algorithm Theoretical Basis Document, Version 2.1. NASA/GSFC, Greenbelt, MD.

Grimmond, S., Blackett, M., Best, M., Baik, J.-j., Belcher, S., Bohnenstengel, S.I., et al., 2010. The international urban energy balance models comparison project: first results from phase 1. Journal of Applied Meteorology and Climatology 49 (6), 1268–1292.

Herold, M., Schiefer, S., Hostert, P., Roberts, D.A., 2006. Applying imaging spectrometry in urban areas. In: Weng, Q., Quattrochi, D. (Eds.), Urban Remote Sensing. CRC Press, Florida, pp. 137–162.

Jensen, J.R., 2007. Remote Sensing of the Environment, second ed. Pearson Education, Inc., USA.

Johnson, G.L., Oke, T.R., Lyons, T.J., Steyn, D.G., Watson, I.D., Voogt, J.A., 1991. Simulation of surface urban heat islands under 'ideal' conditions at night. Part 1: theory and tests against field data. Boundary Layer Meteorology 56 (3), 275–294.

Johnson, G.L., Davis, J.M., Karl, T.R., McNab, A.L., Tarpley, J.D., Bloomfield, P., 1993. The use of polar-orbiting satellite sounding data to estimate rural maximum and minimum temperatures. Journal of Applied Meteorology 32 (5), 857–870.

Kawashima, S., Ishida, T., Minomura, M., Miura, T., 2000. Relations between surface temperature and air temperature on a local scale during winter nights. Journal of Applied Meteorology 39 (9), 1570–1579.

Leung, Y.K., Yeung, K.H., Ginn, E.W.L., Leung, W.M., 2004. Climate Change in Hong Kong. Technical Note 107, Hong Kong Special Administrative Region Government.

Leung, Y.K., Yip, K.M., Yeung, K.H., 2008. Relationship between thermal index and mortality in Hong Kong. Meteorological Applications 15 (3), 399–409.

McCarthy, M.P., Best, M.J., Betts, R.A., 2010. Climate change in cities due to global warming and urban effects. Geophysical Research Letters 37, L09705. http://dx.doi.org/10.1029/2010GL042845.

Mills, G.M., 1993. Simulation of the energy budget of an urban canyon – I. Model structure and sensitivity test. Atmospheric Environment 27 (2), 157–170.

Murphy, J.M., Hall, M.H., Hall, C.A.S., Heisler, G.M., 2011. The relationship between land cover and the urban heat island in northeastern Puerto Rico. International Journal of Climatology 31 (8), 1222–1239.

Ng, E., 2009. Wind and heat environment in densely built urban areas in Hong Kong. Global Environmental Research 13 (2), 169–178.

Nichol, J.E., 1998. Visualisation of urban surface temperatures derived from satellite images. International Journal of Remote Sensing, UK 19 (9), 1639–1649.

Nichol, J., 2009. An emissivity modulation method for spatial enhancement of thermal satellite images in urban heat island analysis. Photogrammetric Engineering & Remote Sensing 75 (5), 547–556.

Nichol, J.E., Fung, W.Y., Lam, K.S., Wong, M.S., 2009. Urban heat island diagnosis using ASTER satellite images and 'in situ' air temperature. Atmospheric Research 94 (2), 276–284.

Oke, T.R., 1973. City size and the urban heat island. Atmospheric Environment 7 (8), 769–779.

Oke, T.R., 2004. Initial Guidance to Obtain Representative Meteorological Observations at Urban Sites. IOM Report 81, World Meteorological Organization, Geneva.

Oke, T.R., Johnson, G.T., Steyn, D.G., Watson, I.D., 1991. Simulation of surface urban heat islands under 'ideal' conditions at night. Part 2: diagnosis of causation. Boundary Layer Meteorology 56 (4), 339–358.

Park, H.-S., 1986. Features of the heat island in Seoul and its surrounding cities. Atmospheric Environment 20 (10), 1859–1866.

Pascal, M., Laaidi, K., Ledrans, M., Baffert, E., Caserio-Schonemann, C., Le Tertre, A., Manach, J., Medina, S., Rudant, J., Empereur-Bissonnet, P., 2006. France's heat health watch warning system. International Journal of Biometeorology 50 (3), 144–153.

Robine, J.M., Cheung, S., Le Roy, S., Van Oyen, H., Griffiths, C., Michel, J.P., Herrmann, F.R., 2008. Death toll exceeded 70,000 in Europe during the summer of 2003. Comptes Rendus Biologies 331 (2), 171178.

Sabins, F.F., 1997. Remote Sensing: Principles and Interpretation, third ed. W.H. Freeman, New York.

Schmid, H.-P., 1997. Experimental design for flux measurements: matching scales of observation and fluxes. Agricultural and Forest Meteorology 87 (2–3), 1221–1231.

Stoll, M.J., Brazel, A.J., 1992. Surface–air temperature relationships in the urban environment of Phoenix, Arizona. Physical Geography 13 (2), 160–179.

Vandentorren, S., Bretin, P., Zeghnoun, A., MandereauBruno, L., Croisier, A., 2006. August 2003 heat wave in France: risk factors for death of elderly people living at home. European Journal of Public Health 16 (6), 583–591 (WHO Europe).

Voogt, J.A., Oke, T.R., 1997. Complete urban surface temperatures. Journal of Applied Meteorology 36 (9), 1117–1132.

Voogt, J.A., Oke, T.R., 2003. Thermal remote sensing of urban climates. Remote Sensing of Environment 86 (3), 370–384.

WMO, 2008. WMO Guide Tometeorological Instruments and Methods of Observation, seventh ed., WMO-No 8 (Part 2 Chapter 11). <http://www.wmo.int/pages/prog/www/IMOP/publications/CIMO-Guide/CIMOGuide-7thEdition-2008.html>.

Wong, M.S., Nichol, J.E., Ng, Y.E., 2011. A study of the "wall effect" caused by proliferation of high-rise buildings using GIS techniques. Landscape and Urban Planning 102, 245–253.

Yamashita, S., Sekine, K., et al., 1986. On relationships between heat island and sky view factor in the cities of Tama River Basin, Japan. Atmospheric Environment 20 (4), 681–686.